Interfacial growth of MOF-derived layered double hydroxide nanosheets on graphene slab towards fabrication of multifunctional epoxy nanocomposites

Ye-Tang Pan, Jintao Wan, Xuanliang Zhao, Cheng Li, De-Yi Wang

PII: S1385-8947(17)31400-6
DOI: http://dx.doi.org/10.1016/j.cej.2017.08.059
Reference: CEJ 17510

To appear in: *Chemical Engineering Journal*

Received Date: 7 May 2017
Revised Date: 10 August 2017
Accepted Date: 13 August 2017

Please cite this article as: Y-T. Pan, J. Wan, X. Zhao, C. Li, D-Y. Wang, Interfacial growth of MOF-derived layered double hydroxide nanosheets on graphene slab towards fabrication of multifunctional epoxy nanocomposites, *Chemical Engineering Journal* (2017), doi: http://dx.doi.org/10.1016/j.cej.2017.08.059

Interfacial growth of MOF-derived layered double hydroxide nanosheets on graphene slab towards fabrication of multifunctional epoxy nanocomposites

Ye-Tang Pan,[a] *Jintao Wan,*[a] *Xuanliang Zhao,*[a, b] *Cheng Li*[a,c] *and De-Yi Wang**[a]

[a]IMDEA Materials Institute, C/Eric Kandel, 2, 28906 Getafe, Madrid, Spain

[b]School of Materials Science and Engineering, Tsinghua University, Beijing 100084, China

[c]State Key Laboratory of Chemical Engineering, College of Chemical and Biological Engineering, Zhejiang University, Zheda Road 38, Hangzhou 310027, China

ABSTRACT: In order to develop safe electrical insulating epoxy nanocomposites with fast heat dissipation and low fire hazard, a "3D fabrication method" was proposed to employ acid-sensitive metal organic framework (MOF) as precursor to construct sandwich-type three-dimensional (3D) graphene/layered double hydroxide (LDH) hybrid structure (rGO@LDH) with NiCo-LDH platelets standing vertically or lying horizontally on both sides of graphene nanosheets which act as a high-performance nanofiller in epoxy nanocomposite. The LDH sheath encased the surface of graphene, impeding electrical conduction and effectively generating a 3D phonon transport channel prone to fast heat dissipation. A 2 wt.% rGO@LDH-treated epoxy nanocomposite sustained an electrical resistivity of 1.21×10^{14} Ω cm and its thermal conductivity was 0.421 W m^{-1} K^{-1}, 81.4% higher than that of pure epoxy resin. Likewise, thanks to the physical barrier and catalytic effects of rGO@LDH, the nanocomposite had low fire hazard indicated by cone calorimeter data showing that peak of heat release rate and total smoke production decreased strikingly compared with those of the pristine one. Moreover, the thermal stability and tensile strength of the nanocomposite were also enhanced in the presence of rGO@LDH. This work advances progress on the development of highly safe multifunctional epoxy nanocomposite for practical use.

KEYWORDS: Graphene; Metal organic framework; Layered double hydroxide; Epoxy nanocomposites

INTRODUCTION

Thermal management with rapid heat dissipation is of paramount importance to cater to the demands of the continued miniaturisation of electronic devices.[1] The heat generated in electronics, optoelectronics, batteries, and so forth caused by a small difference in the operating temperature results in an enormous reduction in the lifespan of the devices.[2] Therefore, the heat needs to be removed efficiently to prevent the malfunction of the device due to overheating. With the help of advantages including high corrosion resistance, light weight and flexibility of the conductivity to adapt to the needs of the application compared with metals and ceramics, recently substantial research was conducted into thermosetting or thermoplastic polymers as thermal interface material. Unfortunately, thermal conductivity of pristine conventional polymer materials is low, which makes it impractical in many fields.[3] Thus, various additives have been incorporated into polymers to improve thermal conductivity. Among these additives, graphene has been proved to be one of the most effective thermally conductive fillers thanks to its large surface area, high thermal conductivity and high aspect ratio 2D structures, which advance the formation of bridges or percolating network as a thermally conducting chain in polymers.[4] Although graphene has so many merits, it is subject to aggregation and forms irreversibly precipitated agglomerate, impeding the uniform dispersion in the polymer matrix and resisting phonon transport at the graphene-polymer interfaces. Moreover, the weak interfacial attraction between the soft polymer and ultra-rigid graphene hinders phonon movement and ruins the thermal conductivity of polymer. In addition, the good electrical conductivity of graphene gives rise to some problems. Achieving efficient long-distance transmission of electric power with minimum losses to highly populated regions requires cables that can withstand a very high voltage, and this can only be fulfilled through highly insulating cable insulations.[5] The epoxy

resin coatings on cable joints and terminals demand high insulation grade to reduce power losses and safety problems. Epoxy resin is inherently electrical insulating. However, the epoxy-based thermal interfacial materials with modified graphene as additives are unable to promise that since nearly all the modification methods reported for graphene cannot ensure the uniform cover on graphene sheets by the decorated insulating particles, leading to graphene sheets in contact with one another by the exposed bare surfaces enabling the transportation of electrons, which restricts their applications. Hsiao et al. prepared the epoxy nanocomposites with reduced graphene oxide-silica hybrid nanosheets and found that the product was thermal conductive and electrical insulating in the presence of the modified graphene with an adding amount lower than 0.5 wt.%, yet the electrical resistivity decreased when the adding amount reached 1 wt.% because some parts of the graphene surfaces were not covered by silica and in touch with one another as the author supposed.[6] As a result, it is challenging to produce thermally conductive graphene-polymer nanocomposites without sacrificing the electrically insulating property.

Layered double hydroxides (LDH) are 2D layered anionic clays generally expressed as $[M^{II}_{1-x}M^{III}_{x}(OH)_2](A^{n-})^{x/n}\cdot mH_2O$ (M^{II} and M^{III} are divalent and trivalent metals respectively, A^{n-} is interlayered anion) widely applied in many areas.[7] The integration of graphene with LDH attracts intensive attention among researchers. The different shapes (from sheet to laminate) and sizes (from micrometers to nanometers) of the graphene to LDH favour the synergistic effects between graphene and LDH, fusing the advantages of both two-dimensional materials. One of the most-investigated hybrid structures is to embed the LDH platelets onto the surface of graphene sheets. Based on the previous reports, there were two combination manners for graphene and LDH. One was LDH platelets lying horizontally along an a, b axis of graphene basal plane (designated as lying LDH) by direct deposition of LDH platelets on graphene scaffold in terms of one-step

coprecipitation method conforming to thermodynamic stability.[8-10] According to this method, LDH platelets exhibited a poor distribution on the graphene surface and aggregated severely, contributing to negligible improvement of the specific surface area and exposure of plentiful void space on graphene surface. The other one on the basis of in situ growth method seemingly avoided the above drawbacks by placing the LDH standing vertically or at an angle along the c axis of graphene basal plane on the graphene scaffold (designated as standing LDH). Xu et al. first coated AlOOH colloids onto graphene surfaces and subsequently grew LDH perpendicularly on the surface of graphene.[11] Notwithstanding, this method facilitated the uniform dispersion of LDH on graphene and furnished a high specific surface for this 3D composite. The void space still appeared substantially on the edge of graphene nanosheets. To the best of our knowledge, there is no report on the uniformly wrapped graphene nanosheets by LDH platelets lying and standing on both sides.

Herein we conceived a tactful synthetic route that employed metal organic framework (MOF) nanocrystals as sacrificial precursors. The zeolitic imidazolate framework (ZIF) as a classic example of MOF has been proven to be an ideal template to prepare hollow LDH nanocage.[12, 13] Inspired by this, the ZIF-67, which has potential to be etched into the 3D LDH framework, was adopted as precursor to construct both standing and lying LDH nanoflakes on graphene with well-defined interfaces (denoted as rGO@LDH). Since current reports all involved the "surface modification method", in this work a "surface coating method" was proposed. We term this strategy "3D fabrication method" to prepare a sandwich-type nanostructure that graphene sheets (or other two-dimensional derivative materials) were evenly wrapped by intimately arranged standing and lying LDH as a sheath, benefiting to prevent restacking of graphene and the contact between different individual graphene sheets. In light of structure-property relationship, it can be

anticipated that the thermal and electrical features of epoxy nanocomposite in presence of rGO@LDH will be affected strikingly. Meanwhile, the flame retardancy of nanocomposite was also taken into consideration, since the low fire hazard was especially crucial for the epoxy nanocomposites used in the practical application.[14-16] The dynamic mechanical analysis and tensile test were carried out to evaluate the mechanical properties of nanocomposites. We aim to engineer a safe electrical insulating epoxy nanocomposite with fast heat dissipation and low fire hazard.

EXPERIMENTAL SECTION

Materials. Potassium permanganate (ACS reagent, ≥99%, $KMnO_4$), sulfuric acid (ACS reagent, 95.0-98.0%, H_2SO_4), graphite (powder, <20 μm, synthetic), sodium nitrate (reagent grade, ≥99.0%, $NaNO_3$), hydrogen peroxide solution (≥30%, H_2O_2), cobalt (II) nitrate hexahydrate [ACS reagent, ≥98%, $Co(NO_3)_2 \cdot 6H_2O$], 2-methylimidazole (99%, 2-MIM), nickel (II) nitrate hexahydrate [≥98.5%, $Ni(NO_3)_2 \cdot 6H_2O$], methanol (anhydrous, 99.8%) and ethanol (absolute alcohol, without additive, ≥98%) were all purchased from Sigma-Aldrich Chemical Co. Epoxy resin (Epoxydhedraz C) was provided by R&G Faserverbundwerkstoffe GmbH-Germany. Diamino diphenyl sulfone (DDS) was supplied by TCI Chemicals Company.

Preparation of rGO@LDH, rGO and LDH. GO was produced from graphite powders according to the modified Hummers method.[17] 3 g $Co(NO_3)_2 \cdot 6H_2O$ was dissolved into 200 ml methanol. Then 100 mg GO was added into solution and sonicated for 30 min. Another 200 ml methanol solution with 4 g 2-MIM inside was mixed with the above solution quickly and aged for 24 h. The intermediate product (denoted as rGO@ZIF-67) was collected by centrifugation and washed by methanol several times. After drying in a vacuum oven at room temperature, 0.5 g intermediate product was redispersed into 200 ml ethanol. Afterwards, 1.35 g $Ni(NO_3)_2 \cdot 6H_2O$

was added into solution and the solution was stirred for 40 min. The slurry was incubated at 80 °C for 2 days. The final product was collected by centrifugation, washed by deionized water and ethanol several times and dried at room temperature, affording the rGO@LDH nanohybrids. The rGO was obtained by the same way in the absence of metal salts and ligand.[18] The LDH was also prepared without the addition of GO.

Preparation of epoxy nanocomposites. Different weight fractions ranging from 0.5 to 2 wt.% rGO and rGO@LDH were exploited to prepare epoxy nanocomposites. As a control, the epoxy nanocomposite containing 2 wt.% LDH was also prepared. First, the fillers were blended into the epoxy matrix by using a three-roll mix (EXAKT 80E, Germany) for 30 min. The mixture was transferred onto a magnetic stirring apparatus and heated up to 130 °C. Under vigorous stirring, DDS was added into the mixture and then stirred until a homogenous solution was obtained. The bubbles were removed by placing the solution into a vacuum oven at 100 °C for 20 min and then poured into the pre-heated PTFE melds immediately. The curing procedure was appointed as 160 °C 1 h, 180 °C for 2 h and 200 °C for 2 h. After cooling down to room temperature, the epoxy nanocomposites were acquired.

Measurements. Philip X' Pert PRO diffractometer equipped with a Cu Kα tube and Ni filter (λ = 0.15405 nm) was employed to record X-ray diffraction (XRD) patterns. Fourier transform infrared spectroscopy (FT-IR) measurements were gathered on a Nicolet iS50 spectrometer with the transmission mode in the wavenumber range of 4000-400 cm^{-1}. The samples were blended with KBr and pressed into pellets for analysis. Nitrogen adsorption and desorption isotherms at 77 K were obtained on a Micromeritics instrument (ASAP 2010). The specific surface area and the pore size distribution were computed by the Brauner–Emmett–Teller (BET) equation and Barrett–Joyner–Halenda (BJH) model, respectively. Transmission electron microscope (TEM)

analysis was carried out on a Tecnai T20 (FEI company) at 80 kV. The Raman spectra were recorded at ambient temperature on a LeicaDM 2700 microscope with YAG laser (50 mW at 532 nm) and a diffraction grating of 1800 l/mm. X-ray photoelectron spectroscopy (XPS) was studied by an Organic Molecular Beam Epitaxy (OMBE) system and the Al Kα line (hν = 1486.7 eV) was used from an Al anode. Morphology and elemental analysis of the fractured epoxy nanocomposites were investigated by scanning electron microscopy (SEM, EVO MA15 Zeiss) coupled with an energy dispersive X-ray detector (EDX). All the samples were covered by a thin gold layer. Thermogravimetric analysis (TGA) was determined from room temperature to 700 °C, with a heating rate of 10 °C/min in N_2 atmosphere (for graphene oxide and reduced graphene oxide, the heating rate was set as 5 °C/min) with flow speed 90 ml/min using a TA Q50 thermogravimetric analyser. Thermal conductivities of all the samples was measured by the thermal conductivity analyser (C-Therm TCi, C-Therm Technologies Ltd., Fredericton, Canada) at room temperature. Volume electrical resistivities were measured using an ultra-high resistance ohmmeter (6517A, Keithley Instruments Inc.). Fire hazards of samples in a forced-flaming condition were detected on an FTT Cone Calorimeter according to ISO5660 under an external heat flux of 50 kW/m^2 100 × 100 × 4 mm^3 in size. Dynamic mechanical analysis (DMA) was conducted on a Q800 DMA (TA Instruments, USA) from room temperature to 300 °C at a heating rate of 5 °C/min and at a frequency of 1 Hz in the tensile configuration. The tensile tests were carried out by using an INSTRON 5966 dual column tabletop universal testing system according to the ASTM D3039-08 method, at a crosshead speed of 3.0 mm/min.

RESULTS AND DISCUSSION

Characterisation of rGO@LDH. The XRD patterns of GO and rGO@LDH were shown in Fig. S1. The peaks located at 2θ values of 11.5°, 23.0°, 33.7° and 60.0° in the XRD pattern of

rGO@LDH were indexed to (003), (006), (009) and (110) planes of hydrotalcite-like LDH phase, which was consistent with a previous report related to NiCo-LDH.[19, 20] The (002) peak of GO was missing in the rGO@LDH sample, indicating a high dispersion state of GO in the composite due to the damaged face-to-face stacking by the introduction of NiCo-LDH on both sides of graphene sheets.[21] The low intensity of diffraction peaks in rGO@LDH pattern was caused by the disorder in the stacked structure between LDH platelets and graphene nanosheets.[22] The TGA curves of GO, rGO, LDH and rGO@LDH were depicted in Fig. S2. It can be seen that the thermal decomposition of rGO@LDH was delayed compared with GO, but the thermal stability of the as-synthesized sample was still worse than rGO because of the degradation of hydroxides under high temperature. In turn, the residue at 700 °C of rGO@LDH was higher than that of GO caused by the absence of oxygen-containing groups. The content of rGO in the rGO@LDH was around 68 wt.% calculated by the data of TGA curves. The morphology of GO was presented in Fig. 1a and the GO was sheet-like with a number of wrinkles on the surface. The surface of rGO@LDH was considerably rough covered by many platelets, quite distinct from GO (Fig. 1b). In the enlarged TEM image for the edge of rGO@LDH (Fig. 1c), it can be seen that the LDH platelets were either standing perpendicularly or lying horizontally on the surface of graphene. In particular, no bare sites were observed around the margin of graphene nanosheets. The thickness and lateral size of LDH platelets were measured easily from the TEM image as ca. 3 nm and 20 ~ 25 nm, respectively. The dark parts of the sample were ascribed to the wrinkles and folds of graphene where they gathered more LDH platelets than the plain areas. In Fig. 1d, LDH platelets distributed uniformly on a large-area graphene which effectively separated graphene nanosheets from each other and prohibited the aggregation of LDH platelets during processing of epoxy nanocomposites. In the HRTEM image shown in Fig. 1e, the lattice fringe of rGO@LDH was

very clear and the interlayer distance d = 0.370 nm attributed to (006) plane of NiCo-LDH. The corresponding fast fourier transformation (FFT) in the inset specifically revealed the diffraction spots of (003) and (006) planes of the sample. Likewise, the selected area electron diffraction (SAED) pattern of rGO@LDH (Fig. 1f) showed the diffraction rings assigned to (009) and (110) planes of NiCo-LDH in agreement with the XRD results. The second diffraction ring from inside to outside with d value of 0.21 nm was indexed to the (110) plane of rGO.[23] The EDX spectra in Fig. S3 illustrated that Ni and Co elements co-existed in the sample and the atomic ratio of Ni and Co was 2.8:1. In the high angle annular dark field (HAADF) images (Fig. 1g-i), the elemental mapping disclosed that Ni and Co elements evenly scattered all over the sample.

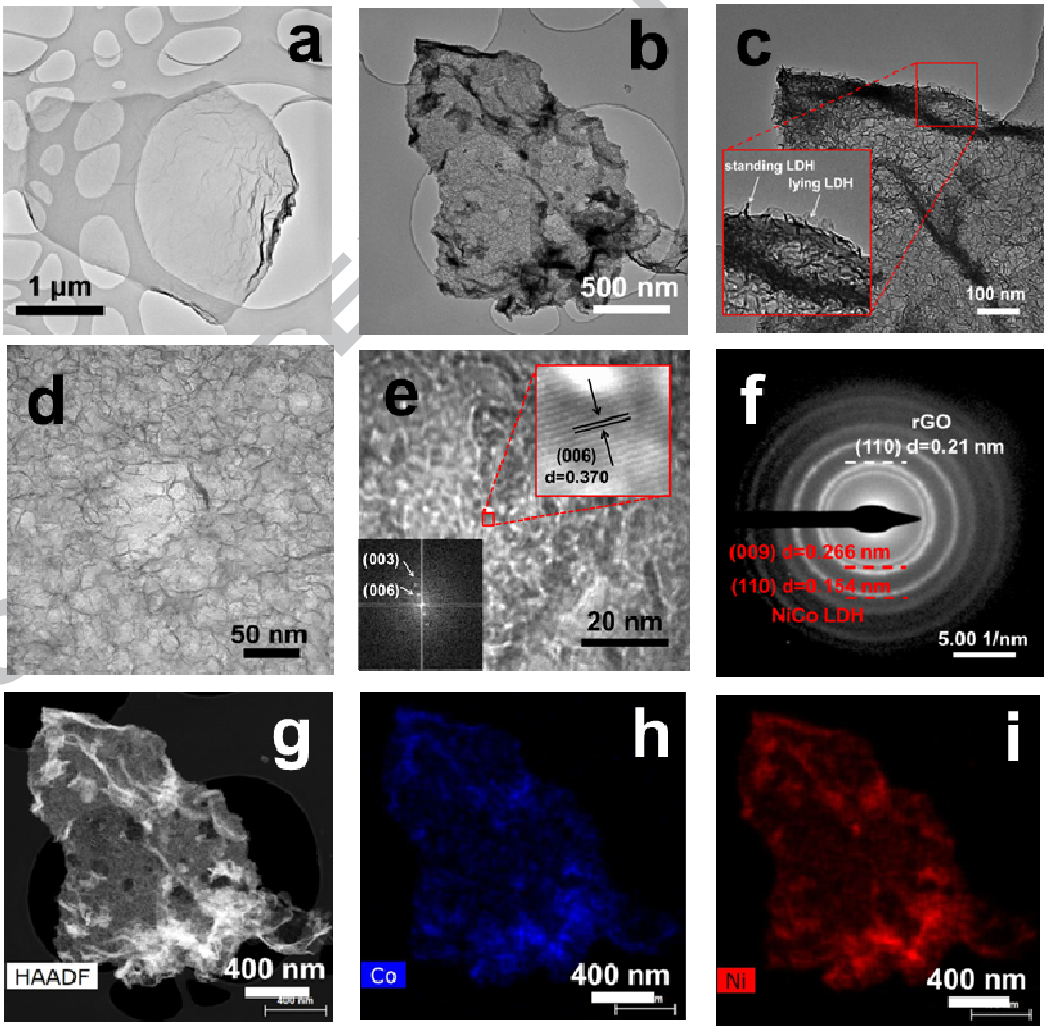

Fig. 1. (a) TEM image of GO; (b) TEM image of rGO@LDH; (c) High magnification TEM image of the edge of rGO@LDH; (d) High magnification TEM image of the center of rGO@LDH; (e) HRTEM image of rGO@LDH (inset: corresponding FFT); (f) SAED pattern of rGO@LDH; (g-i) HAADF image of rGO@LDH and Co, Ni mapping.

The FT-IR spectra of as-synthesized rGO@LDH compared with that of GO provide important information about the oxygen-containing functional group on the surface of graphene and interlayer anions of LDH and hence are very useful to determine the structure of the product. The FT-IR spectra of GO, LDH and rGO@LDH were shown in Fig. 2a. In the spectrum of rGO@LDH, it can be observed that the stretching vibrations of C-O (carboxylic acid) at 1723 cm^{-1}, C-O-C (epoxy) at 1238 cm^{-1} and C-O-H (alkoxy) at 1031 cm^{-1} have disappeared compared with pure GO, indicating the reduction of GO to rGO.[11] Meanwhile, the broad band at 3425 cm^{-1} originated from the O-H streching of water molecules in the system. The bending vibration of water was also detected at around 1630 cm^{-1}. The sharp peak at 1397 cm^{-1} reflected the characteristic band for NO_3^- as the main interlayer anion in the NiCo-LDH.[24] In addition, the bands below 800 cm^{-1} were because of the characteristic bending vibration of Co-O and Ni-O bond, manifesting the formation of NiCo-LDH on graphene.[25-27] Furthermore, the peaks at 1487 cm^{-1} and 1302 cm^{-1} belonged to the stretching vibration of C-H bond and in-plane bending vibration of O-H in ethanol respectively, demonstrating some solution remaining in the sample. Raman spectra is a powerful tool to study the structural changes of graphene materials as it monitors both D band at ca. 1348 cm^{-1} assigned to a breathing mode of κ-point phonons of A_{1g} symmetry and G band at about 1594 cm^{-1} ascribed to the E_{2g} phonon of C sp^2 atoms.[9] In this case (Fig. 2b), the I_D/I_G ratios of GO and rGO@LDH were 0.83 and 0.95, respectively, illustrating the

part reduction of GO and more defects occurred due to the import of LDH fragments on the graphene.[11, 18] The defect sites created by anchorage of ZIF-67 on the graphene surface played a critical role in improving the nucleation of LDH platelets onto graphene nanosheets and inhibiting the agglomeration of LDH nanocrystallites. High specific surface area is one of the textural properties of the designed additive which is well recognised to facilitate the additive to form more interfaces with the polymer matrix, improving the interaction between both. The specific surface area and porous situation of rGO and rGO@LDH were suggested by nitrogen adsorption-desorption isotherms depicted in Fig. S4a, b. It can be seen that both curves presented typical IV isotherms with an H3-type hysteresis loop at $P/P_0>0.5$, indicative of mesopores existing in both samples. The presence of mesopores on the graphene nanosheets in rGO@LDH sample, which was probably due to the etching effect of transitional metal-based nanoparticles.[28] The BET surface area of rGO and rGO@LDH were 128.8 m^2/g and 237.6 m^2/g, respectively. The relatively low surface area of rGO provided the evidence that restacking and aggregation occurred inevitably during the preparation. Nevertheless, for the rGO@LDH, the LDH array grown on the graphene surface worked as a "spacer" to separate the graphene nanosheets. Furthermore, the "3D fabrication method" was prone to decrease the agglomeration of LDH platelets and fabricate a standing LDH array on the surface of graphene, resulting in more exposed LDH platelets and enlarged specific surface area. The rGO@LDH was apt to interact well with epoxy matrix in the nanocomposites thanks to the high surface area and existing mesopores, thereby exhibiting high performance in multiple aspects. The XPS survey scan for rGO@LDH was shown in Fig. S5a, indicating the existence of Ni and Co elements in the sample. In Ni 2p spectrum of rGO@LDH (Fig. 2c), two obvious shakeup satellites close to two spin-orbit doublets were identified as Ni $2p_{1/2}$ and Ni $2p_{3/2}$ signals of Ni^{2+}.[29] In Co 2p XPS spectrum of

rGO@LDH (Fig. 2d), the spin-orbit splitting value of Co $2p_{1/2}$ and Co $2p_{3/2}$ was 15.3 eV, and the satellite line intensity was very low, suggesting the co-existence of Co^{2+} and Co^{3+} in the hybrid.[30]

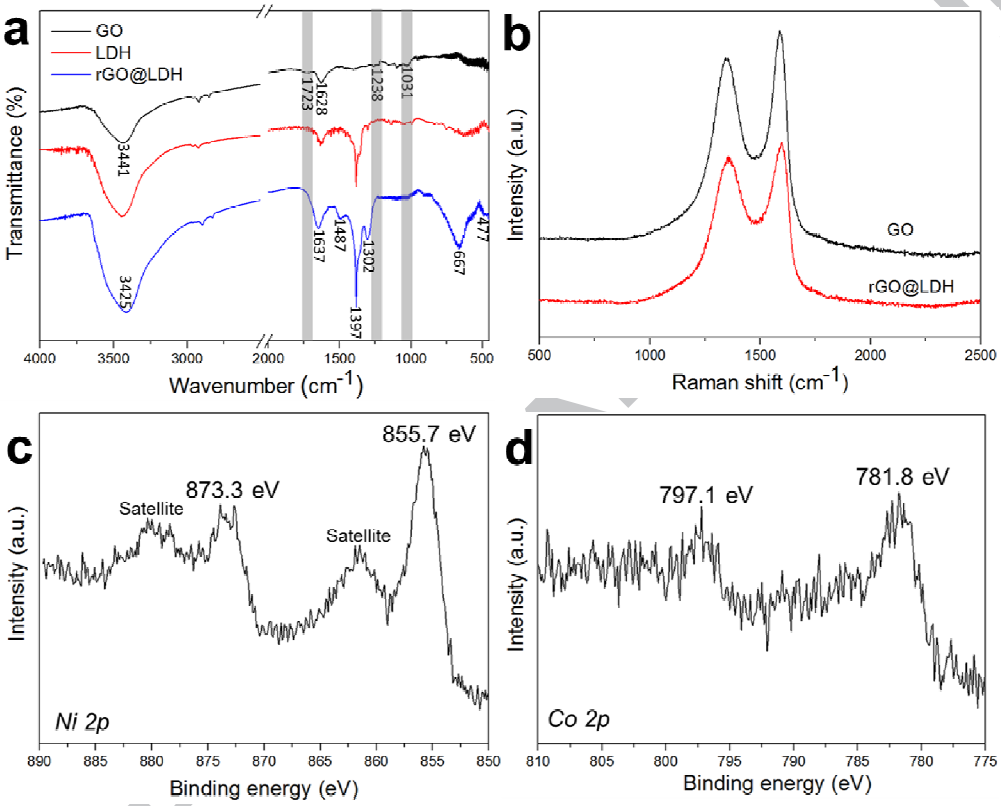

Fig. 2. (a) FT-IR spectra of GO, LDH and rGO@LDH; (b) Raman spectra of GO and rGO@LDH; (c, d) XPS high-resolution spectra of Ni 2p and Co 2p for rGO@LDH.

To investigate the structural evolution process of rGO@LDH, rGO@ZIF-67 and intermediate products at different reaction stages were collected. In Fig. 3a, ZIF-67 polyhedrons were spread uniformly over the whole surface of graphene. Interestingly, the enlarged TEM image obviously indicates the position of the ZIF-67 polyhedrons located on the both sides of the graphene nanosheet. Some exterior ZIF-67 adhered to the nanosheet and other interior ZIF-67 were wrapped by the nanosheet. The EDX results showed that the Co and N elements originated from

ZIF-67 were existing in the sample (Fig. S6). The XRD pattern of rGO@ZIF-67 in Fig. S7 overlapped that of ZIF-67 completely with a little decrease in intensity, demonstrating the successful coating of ZIF-67 on the graphene sheet. In addition, the peak of rGO did not emerge in the rGO@ZIF-67, in line with the XRD results of rGO@LDH. The TEM images of the samples obtained at different time intervals were presented in Fig. 3c and 3d. When the reaction time was 10 min, ZIF-67 polyhedrons were etched into the framework, generating a fibered network on the graphene. The framework continued to decompose into discrete nanosheets accompanying with some broken polyhedrons scattering on the graphene when the reaction time was prolonged to 20 min. The scheme for the synthetic procedure of rGO@LDH was shown in Fig. 3e. Due to the ionisation of the carboxylic acid and phenolic hydroxyl groups, the surface of graphene oxide was usually negatively charged in aqueous solution, therefore Co cation was adsorbed on the graphene by electrostatic force.[21] The GO is responsible for the formation of well dispersed ZIF-67 polyhedrons, with the oxygen-containing functional groups on the surface, functioning as anchoring sites for inducing crystal seed nucleation and growth.[31] Then the ZIF-67 polyhedrons were etched by H^+ derived from the hydrolysis of nickel nitrite into a framework composed of LDH platelets followed by totally collapsing into LDH fragments on the graphene surface. Because of this delicate synthetic route, LDH platelets inherited the 3D structure of ZIF-67 polyhedrons, thereby either standing or lying on the graphene "bed" forming a 3D hybrid structure, in favour of its high performance in the epoxy nanocomposite.

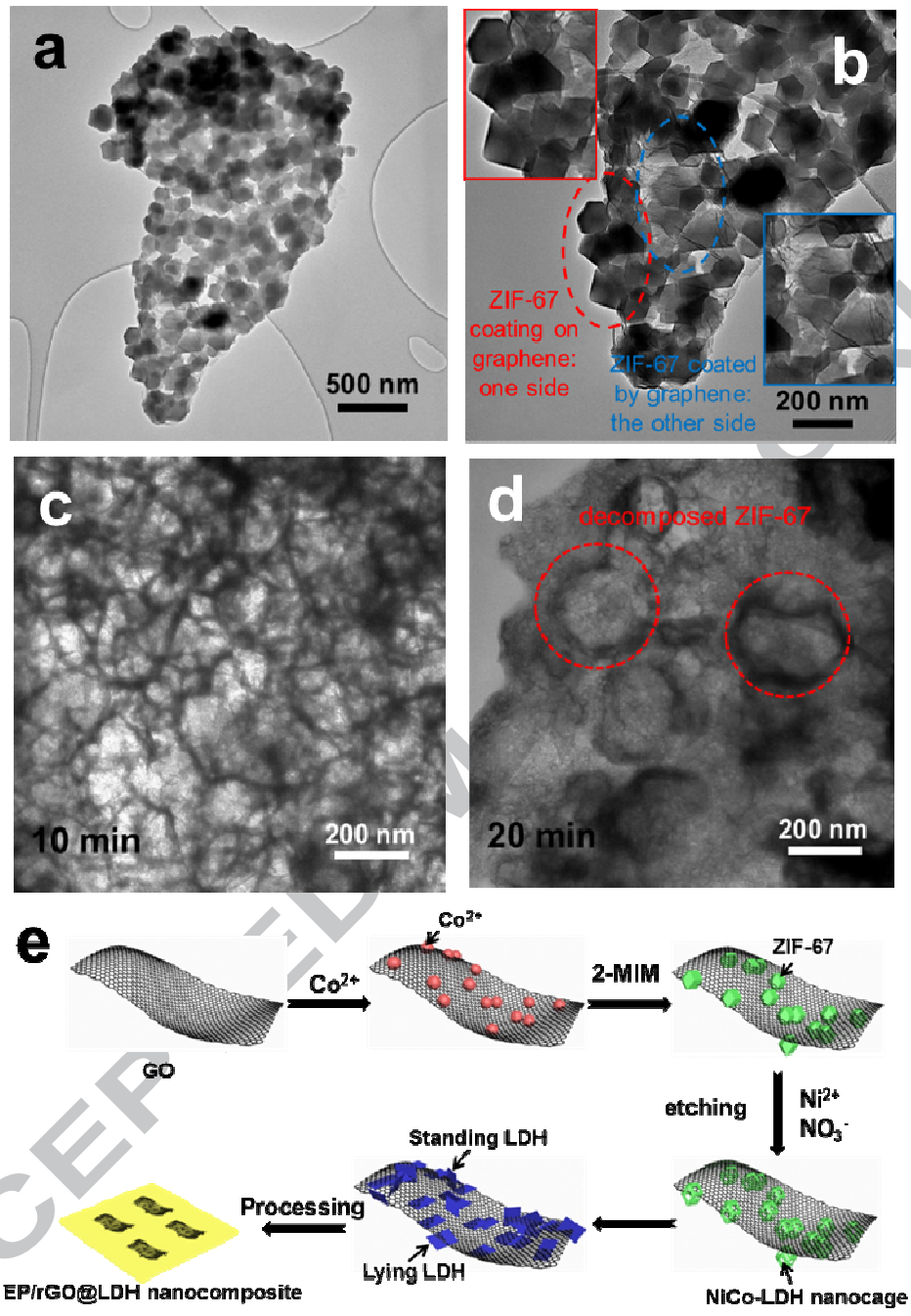

Fig. 3. (a) TEM image of rGO@ZIF-67; (b) High magnification TEM image of rGO@ZIF-67; (c-d) TEM images of the as-synthesized products obtained at different time intervals: 10 min (c), 20 min (d); (e) Schematic illustration of synthesis of rGO@LDH and preparation of EP/rGO@LDH nanocomposites.

Thermal conductivity and electrical resistivity of epoxy nanocomposites. Fig. 4a showed the thermal conductivity of epoxy nanocomposites containing different contents of rGO and rGO@LDH (denoted as EP/rGO and EP/rGO@LDH). The rGO was efficient in improving the thermal stability of epoxy nanocomposite and reached 0.279 W m^{-1} K^{-1} at 0.5 wt.% content, but the efficiency decreased with the content of filler increasing. The possible reason for this is mainly because the occurrence of restacking of graphene nanosheets during the preparation procedure formed agglomeration. It reduced the effective aspect ratio of rGO and acted as a "heat reservoir" restricting heat diffusion.[32] In addition, the weak interfacial attraction between the soft polymer matrix and ultrastiff rGO sheets leading to poor compatibility hampered the phonon transport. Conversely, epoxy nanocomposite containing 2 wt.% rGO@LDH had a thermal conductivity of 0.421 W m^{-1} K^{-1}, which was much higher than that of epoxy resin, because of the low acoustic impedance mismatch between the filler and the polymer matrix. Although the modulus is an intrinsic property of a material, it may be modified by the core-shell and sandwich structured nanomaterials.[6] Incorporating the less stiff two-sided LDH layers as a buffer between the strong graphene and the soft epoxy matrix efficiently reduce the modulus mismatch, decreasing the thermal interfacial resistance between the boundary of inorganic filler and polymer, thus increasing the thermal conductivity of the nanocomposites.[33] In addition, affluent LDH platelets on the rGO not only obstructed the stack of rGO into graphitic structure, affording an integrated thermal transport pathway, but also ameliorated the interfacial adhesion due to the rough surface of modified reduced GO, restricting the motion of epoxy segmental chains.[34] The k and k_0 in the histogram represented the thermal conductivities of the epoxy resin based thermal interfacial materials and epoxy resin, respectively, and $\Delta k = (k-k_0)/k_0$ was the k enhancement. By adding 2 wt.% rGO@LDH, the k enhancement for the epoxy nanocomposite

increased by 81.4% compared with that of the pure epoxy resin, while at the same content, the k enhancement of epoxy nanocomposite in presence of rGO only improved by up to 30.2%. The high thermal conductivity of EP/rGO@LDH was beneficial to the fast heat dissipation from the nanocomposite. Fig. 4b showed the volume electrical resistivities of nanocomposites containing various amounts of rGO and rGO@LDH. Since rGO consisted of π-bonds with high aspect ratio conducive to the transportation of electrons through the π-bonds, epoxy nanocomposite with rGO possessed high thermal conduction. The percolation threshold value for EP/rGO sample was below 0.5 wt.% content on account of a steep decrease within this range in the curve. Around this content, rGO nanosheets inside the nanocomposite formed a conductive network in the polymer matrix leading to improved electrical conductivity of the nanocomposites. The volume electrical resistivity of the nanocomposites decreased sharply with the loading of rGO increasing from 0 to 0.5 wt.%, varying about eight orders of magnitude, from 1.87×10^{15} Ω cm to 6.23×10^{7} Ω cm when the filler content reached 0.5 wt.%. Then the electrical resistivity improved slightly by increasing the amount of rGO because of the inevitable agglomeration of enlarged amount rGO sheets during the process of epoxy nanocomposites. After encasing the graphene nanosheets into an LDH sheath, rGO@LDH provided limited change to the electrical resistivity of epoxy nanocomposites. The electrical resistivity of epoxy nanocomposite incorporated with 2 wt.% rGO@LDH remained at 1.21×10^{14} Ω cm, similar to that of the neat epoxy resin, still locating in the insulation area. The percolation threshold was not observed in the steady curve of epoxy nanocomposite containing rGO@LDH with the loading amount up to 2 wt.%, demonstrating that the entire covering of the insulating LDH layer prevented the electron transport by the underlying graphene nanosheets. This indicates that the LDH layer on the graphene surface sensibly hampered the formation of electrical paths within the nanocomposites

because LDH platelets disrupted conjugating electron transport and augmented the tunneling energy barrier.

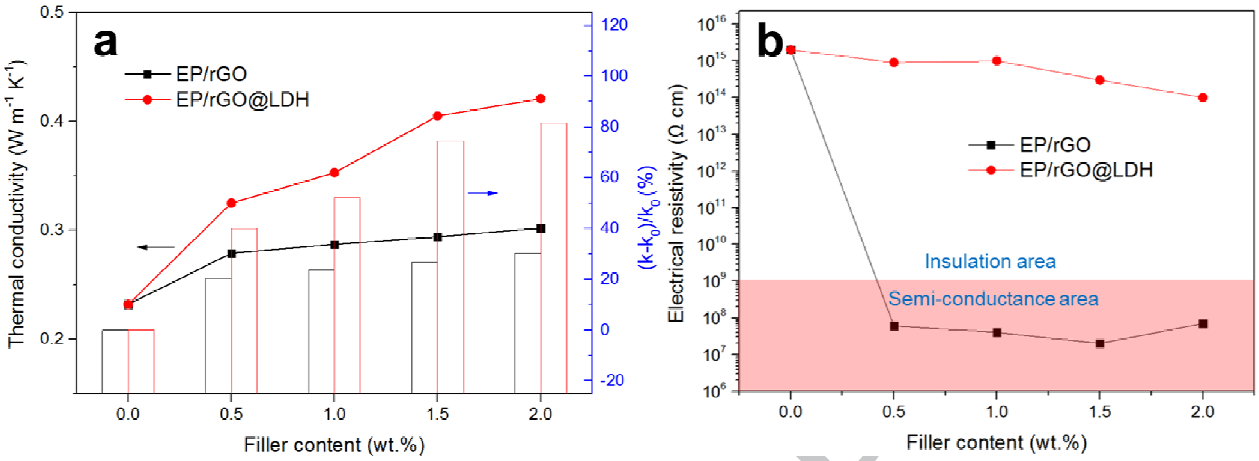

Fig. 4. (a) Thermal conductivity (point plot) and enhancement (bar graph) and (b) electrical resistivities of epoxy nanocomposites containing different contents of rGO and rGO@LDH.

Fire behaviour of epoxy nanocomposites. The fire behaviour of polymer nanocomposites is of great importance to estimate the fire safety of materials. The cone calorimeter test is a widely used and accepted measurement for determining the heat release rate (HRR), total heat release (THR) and total smoke production (TSP) of materials during combustion.[35] Therefore, the fire hazard of EP containing 2 wt.% rGO and 2 wt.% rGO@LDH (denoted as EP/2% rGO and EP/2% rGO@LDH) were evaluated by cone calorimeter. As a control, EP containing 2 wt.% LDH (denoted as EP/2% LDH) was also taken into consideration. The HRR and TSP curves were shown in Fig. 5 and the results were summarised in Table 1. In Fig. 5a, neat EP burned fiercely once it was ignited and exhibited high HRR with the peak value of 961 kW/m^2. The addition of rGO contributed to vanishing the HRR reduction to the polymer nanocomposite irrespective of delaying time to ignition slightly. The peak of HRR (PHRR) for EP/2% rGO was 928 ± 15 kW/m^2, nearly the same to that of the neat one. The addition of LDH decreased the PHRR and

THR of the sample to 554 ± 11 kW/m^2 and 84 ± 2 MJ/m^2, respectively. Of note, with the help of rGO@LDH, the PHRR reduced to 327 ± 23 kW/m^2, 65.9% decrease compared with that of the EP without rGO@LDH. Meanwhile, the THR value also decreased from 96 MJ/m^2 of pure EP to 80 ± 2 MJ/m^2 of EP/2% rGO@LDH. TSP is an indispensable parameter to decide the smoke hazard caused by materials during burning. The rGO was helpful in decreasing the TSP value of the nanocomposite, but the LDH coated graphene was more efficient than the unmodified one and reduced the TSP value from 30 ± 1 m^2 to 21 ± 1 m^2 compared with the pristine EP. Also, the introduction of rGO@LDH afforded the highest char yield among all samples. The digital photos of residue shown in Fig. 5c reflected that the char of the sample containing rGO@LDH was more intact and compact compared with the other two samples. The negligible effect of rGO on fire performance of epoxy nanocomposite illustrated the poor dispersion of the filler in the polymer matrix caused by the severe restacking of rGO nanosheets. The low fire hazard of EP/2% rGO@LDH was probably due to the catalytic effect of transitional metals, nickel and cobalt in the LDH.[36, 37] It availably facilitated the char formation to create a barrier effect on the surface of the polymer, slowing down the heat and mass transfer between gas and condensed phases and protecting the underlying material from further combustion.[38, 39]

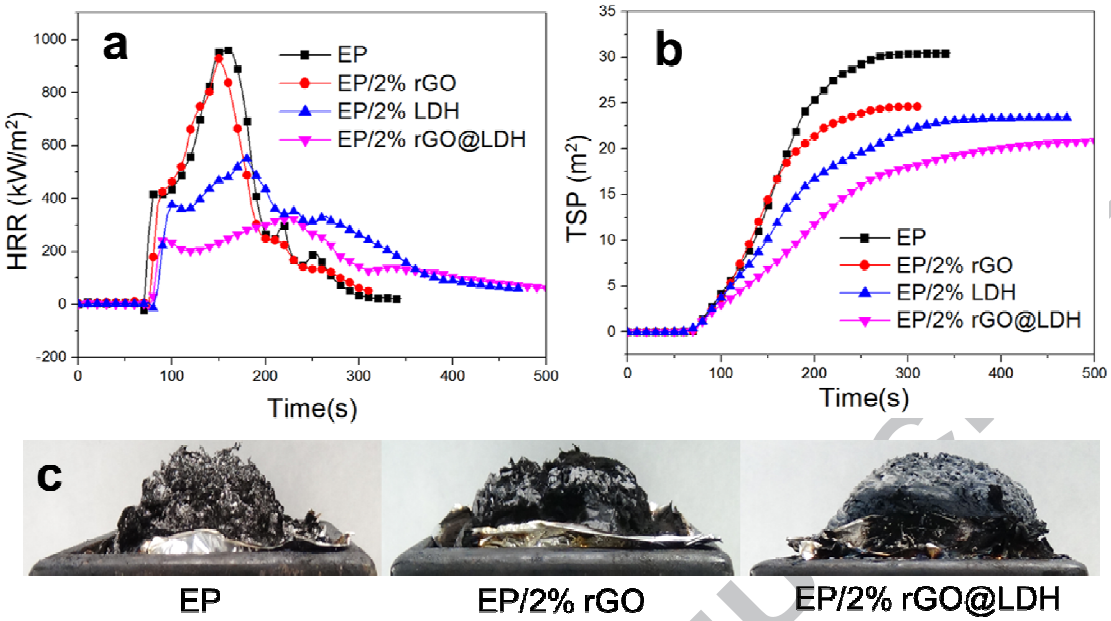

Fig. 5. Cone calorimeter data of epoxy nanocomposites: (a) heat release rate curves; (b) total smoke production curves; (c) Digital photos of char residue.

Table 1. Cone data summary for epoxy nanocomposites.

Sample	PHRR (kW/m^2)	THR (MJ/m^2)	TSP (m^2)	Residue (%)
EP	961 ± 12	96 ± 3	30 ± 1	11.9 ± 0.9
EP/2% rGO	928 ± 15	87 ± 2	24 ± 1	13.1 ± 1.1
EP/2% LDH	554 ± 11	84 ± 2	23 ± 1	17.3 ± 0.7
EP/2% rGO@LDH	327 ± 23	80 ± 2	21 ± 1	21.6 ± 2.1

Thermal stability and fractured surface characteristic of epoxy nanocomposites. The thermogravimetric analysis was performed to study the thermal stability of epoxy nanocomposites. The TG profiles for epoxy and its composites as a function of temperature at a heating rate of 10 °C/min under N_2 atmosphere were shown in Fig. 6. All the thermograms displayed a one-stage degradation process which corresponded to the decomposition of the

macromolecular chains.[40] The onset decomposition temperature ($T_{5\%}$) referred to the temperature at which the weight loss of the sample was 5%. From the data in the table in the inset, it can be easily observed that EP/2% rGO and EP/2% rGO@LDH showed an increment in $T_{5\%}$ compared with the pure one. This improvement in thermal stability could be originated from the so-called "tortuous path" effect of graphene, which retards the permeation of heat and the escape of volatile degradation products.[41] Moreover, the sample with rGO@LDH had the highest residue of 19.7% at 700 °C, whereas for EP and EP/2% rGO, the residue was 14.3% and 16.1%, respectively, suggesting that rGO@LDH functionalised as an effective barrier to inhibit the mass loss during the thermal degradation process and promoted the char formation which was a requisite for a good flame retardant for epoxy nanocomposites.

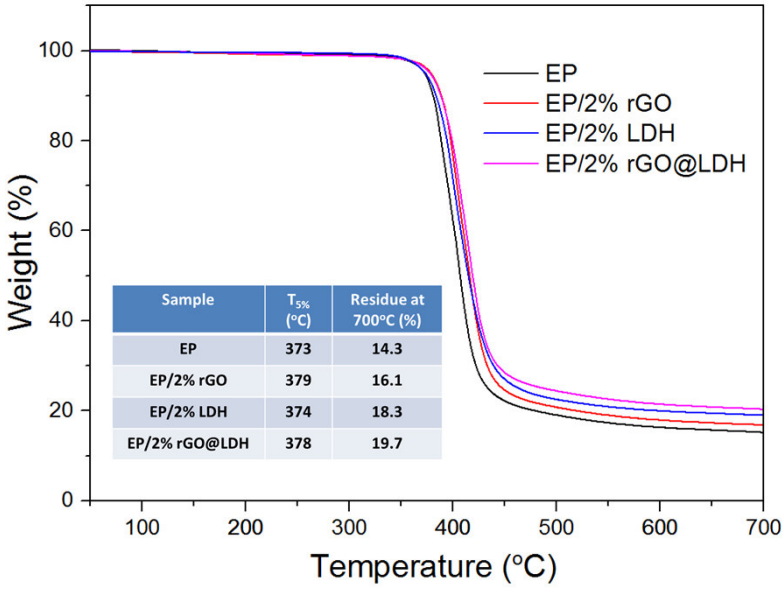

Fig. 6. TGA profiles for epoxy and its composites as a function of temperature under nitrogen atmosphere.

It is well recognized that the interfacial compatibility between nanofillers and polymer matrix plays a vital role in enhancing the integrated performance of nanocomposites.[42] The cryo-fractured surface microstructures of EP and its nanocomposites were studied by SEM shown in

Fig. 7. The neat EP emerged on a smooth surface with no feature in Fig. 7a. When 2 wt.% rGO was added into the composite, rGO nanosheets were apt to form large agglomerations in the system and restacked together severely. Comparatively, dispersion of the additive changed better for the case of composite with 2 wt.% rGO@LDH in Fig. 7c. The rGO@LDH resided on the surface of the composite were much smaller than the agglomeration of rGO. The elemental mapping of the EP/2% rGO@LDH sample in Fig. S8 indicated that the particle on the surface was assigned to rGO@LDH in terms of the well-distributed nickel and cobalt elements within the particle. The smaller grain size and rougher surface of rGO@LDH compared with rGO strikingly increased the interfacial adhesion between the additive and EP matrix, promising the enhancement for properties of the nanocomposite.

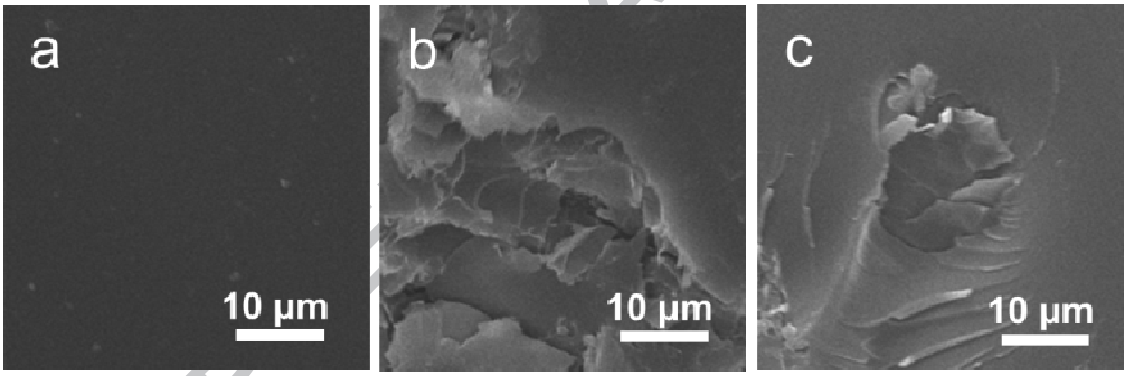

Fig. 7. SEM images of the fractured sections of (a) neat EP, (b) EP/2% rGO and (c) EP/2% rGO@LDH.

Mechanical properties of epoxy nanocomposites. Dynamic mechanical analysis provides the information of the storage modulus and tan δ as the function of testing temperature. In Fig. 8a, the values of storage modulus in the glass state section of neat EP and EP/2% rGO were nearly the same, while the EP/2% rGO@LDH showed a much higher value, caused by the confinement and relatively uniform distribution of the rGO@LDH in the polymer matrix.[43] Moreover, the

steep decrease of storage modulus during the glass transition process was delayed by 5 °C in EP/2% rGO@LDH compared with pristine EP. The enhanced thermo-mechanical properties were induced by 0the network structure generated by the rGO@LDH sheets in the composite, which restrained the mobility of the main chains of the epoxy resin. In Fig. 8b, the peak of tan δ indicated the glass transition temperature T_g. The T_g value for EP/2% rGO@LDH was a little higher than that of pure EP because of the lamellar barrier effect of nano-flakes restricting the segment motion of polymer chains in the matrix.[44] On the contrary, the obvious decrease of T_g for the sample bearing rGO seemingly occurred due to the inevitable agglomeration during the processing of the composite, manifesting its worse dispersion in the polymer matrix owing to the restacking without the support of LDH platelets.

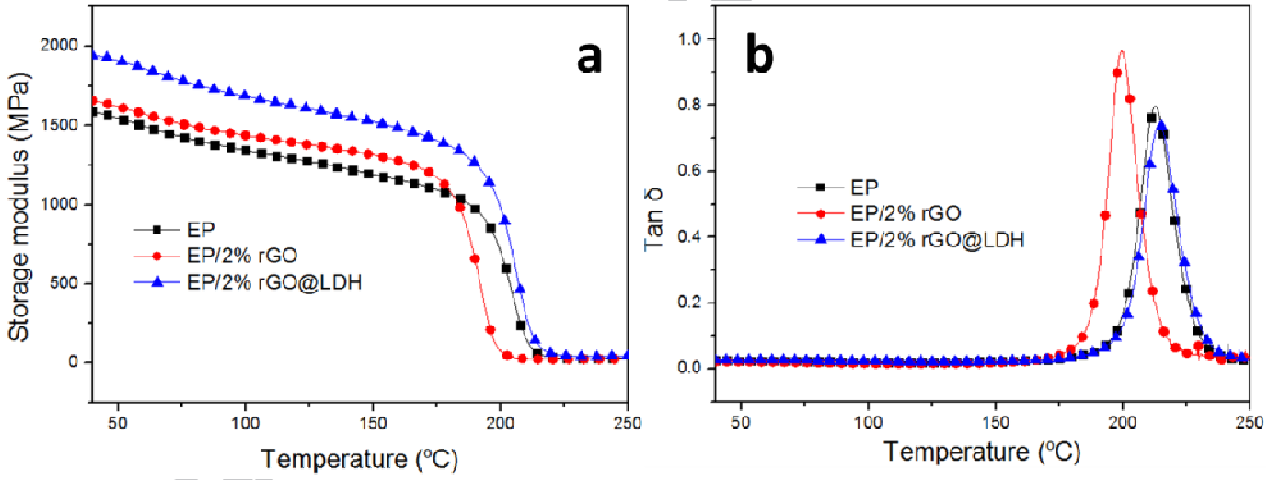

Fig. 8. Dynamic mechanical curves for EP, EP/2% rGO and EP/2% rGO@LDH composites: (a) storage modulus; (b) tan δ.

In order to gain more information about the interfacial adhesion between the nanoparticles and the epoxy matrix, tensile tests were carried out. The tensile stress curves as a function of strain were shown in Fig. 9. Both 2 wt.% rGO and rGO@LDH filled nanocomposites displayed higher tensile strength than the pure one. The enhanced tensile was attributed to the micro-crazing

initiated by the nanosheets, which could relieve the stress state and limit the void formation in the bulk polymer.[45, 46] The curves in presence of rGO and rGO@LDH showed no appearance of yield ascribing to brittle failure, which were the same as that of the cured pure epoxy.[47] The similar elongation at break of EP/2% rGO@LDH compared with that of pristine EP proved the better dispersion of discrete rGO@LDH than the aggregated restacking rGO in the polymer matrix. The Young's modulus after incorporating the additives increased from 2.2 GPa to more than 3.0 GPa on account of the intrinsic stiffness of graphene-based materials.

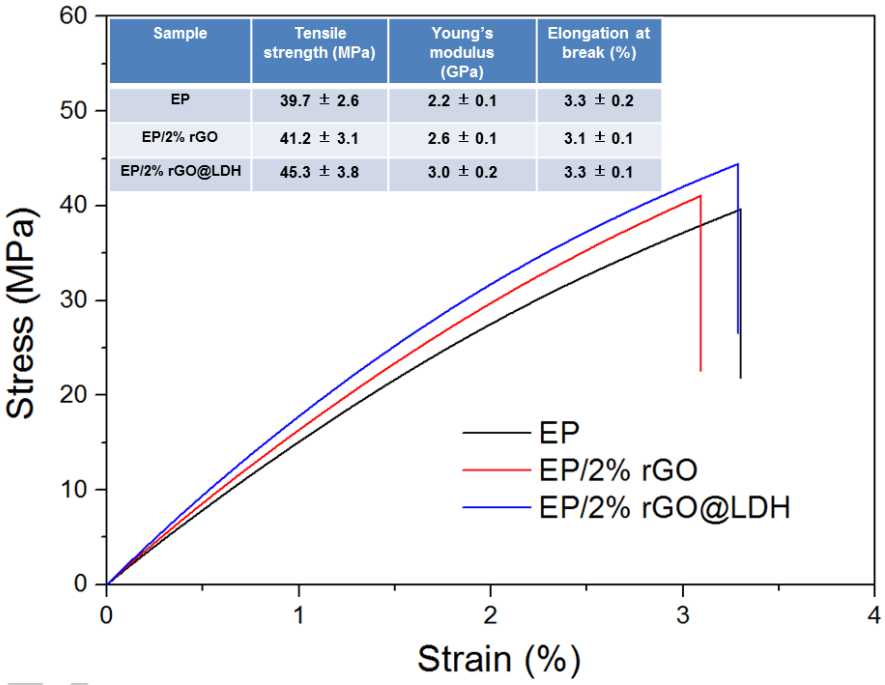

Fig. 9. Stress-strain curves of epoxy nanocomposites filled with 2 wt.% rGO and 2 wt.% rGO@LDH.

CONCLUSIONS

In this work, a sandwich-type 3D nanostructure was assembled via coating NiCo-LDH platelets derived from MOF on the graphene nanosheets. During the modification, concurrent reduction of graphene oxide was accomplished. The fascinating structure of the as-synthesized sample was

characterized as all sided by various measurements. The well-connected constituents of the hybrid endowed the epoxy nanocomposite with enhanced thermal conductivity and flame retardancy, while the nanocomposite was still an insulator. Epoxy nanocomposite with 2 wt.% rGO@LDH retained an electrical resistivity of 1.21×10^{14} Ω cm and its thermal conductivity was 0.421 W m^{-1} K^{-1}. Meanwhile, the peak of heat release rate and total smoke production descended by 65.9% and 16.7% respectively compared with those of neat epoxy. The thermal stability and tensile strength of the epoxy nanocomposite in presence of rGO@LDH were improved simultaneously. The proposed "3D fabrication method" to prepare stereo LDH/rGO hybrid offers blueprints for designing highly safe electrical insulating epoxy nanocomposites with fast heat dissipation and low fire hazard for practical use.

ASSOCIATED CONTENT

Supporting Information. The following files are available free of charge.

XRD patterns, TGA profiles, N_2 adsorption/desorption isotherms, XPS spectra, EDX spectra and elemental mapping.

AUTHOR INFORMATION

Corresponding Author

* E-mail address: deyi.wang@imdea.org

ACKNOWLEDGMENT

This research is partly funded by the European Commission under the 7th Framework Programme (Marie Curie Career Integration Grant, ECOFIRE-NANO), Spanish Ministry of

Economy and Competitiveness (MINECO) under Ramón y Cajal fellowship (RYC-2012-10737), PhD program funded by China Scholarship Council (201306120037) and COST Action CM1302(Smart Inorganic Polymers, SIPs).

REFERENCES

(1) Shen, X.; Wang, Z.; Wu, Y.; Liu, X.; He, Y.-B.; Kim, J.-K., Multilayer Graphene Enables Higher Efficiency in Improving Thermal Conductivities of Graphene/Epoxy Composites. *Nano Lett.* **2016,** *16*, 3585-3593.
(2) Im, H.; Kim, J., Thermal Conductivity of a Graphene Oxide–Carbon Nanotube Hybrid/Epoxy Composite. *Carbon* **2012,** *50*, 5429-5440.
(3) Eksik, O.; Bartolucci, S. F.; Gupta, T.; Fard, H.; Borca-Tasciuc, T.; Koratkar, N., A Novel Approach to Enhance the Thermal Conductivity of Epoxy Nanocomposites Using Graphene Core–Shell Additives. *Carbon* **2016,** *101*, 239-244.
(4) Yavari, F.; Fard, H. R.; Pashayi, K.; Rafiee, M. A.; Zamiri, A.; Yu, Z.; Ozisik, R.; Borca-Tasciuc, T.; Koratkar, N., Enhanced Thermal Conductivity in a Nanostructured Phase Change Composite Due to Low Concentration Graphene Additives. *J. Phys. Chem. C* **2011,** *115*, 8753-8758.
(5) Pourrahimi, A. M.; Hoang, T. A.; Liu, D.; Pallon, L. K. H.; Gubanski, S.; Olsson, R. T.; Gedde, U. W.; Hedenqvist, M. S., Highly Efficient Interfaces in Nanocomposites Based on Polyethylene and ZnO Nano/Hierarchical Particles: A Novel Approach toward Ultralow Electrical Conductivity Insulations. *Adv. Mater.* **2016,** *28*, 8651-8657.
(6) Hsiao, M.-C.; Ma, C.-C. M.; Chiang, J.-C.; Ho, K.-K.; Chou, T.-Y.; Xie, X.; Tsai, C.-H.; Chang, L.-H.; Hsieh, C.-K., Thermally Conductive and Electrically Insulating Epoxy Nanocomposites with Thermally Reduced Graphene Oxide–Silica Hybrid Nanosheets. *Nanoscale* **2013,** *5*, 5863-5871.
(7) Dou, Y.; Zhang, S.; Pan, T.; Xu, S.; Zhou, A.; Pu, M.; Yan, H.; Han, J.; Wei, M.; Evans, D. G., TiO_2@Layered Double Hydroxide Core–Shell Nanospheres with Largely Enhanced Photocatalytic Activity toward O_2 Generation. *Adv. Funct. Mater.* **2015,** *25*, 2243-2249.
(8) Garcia-Gallastegui, A.; Iruretagoyena, D.; Gouvea, V.; Mokhtar, M.; Asiri, A. M.; Basahel, S. N.; Al-Thabaiti, S. A.; Alyoubi, A. O.; Chadwick, D.; Shaffer, M. S. P., Graphene Oxide as Support for Layered Double Hydroxides: Enhancing the CO_2 Adsorption Capacity. *Chem. Mater.* **2012,** *24*, 4531-4539.
(9) Li, M.; Zhu, J. E.; Zhang, L.; Chen, X.; Zhang, H.; Zhang, F.; Xu, S.; Evans, D. G., Facile Synthesis of Nial-Layered Double Hydroxide/Graphene Hybrid with Enhanced Electrochemical Properties for Detection of Dopamine. *Nanoscale* **2011,** *3*, 4240-4246.
(10) Wang, X.; Zhou, S.; Xing, W.; Yu, B.; Feng, X.; Song, L.; Hu, Y., Self-Assembly of Ni–Fe Layered Double Hydroxide/Graphene Hybrids for Reducing Fire Hazard in Epoxy Composites. *J. Mater. Chem. A* **2013,** *1*, 4383-4390.
(11) Xu, J.; Gai, S.; He, F.; Niu, N.; Gao, P.; Chen, Y.; Yang, P., A Sandwich-Type Three-Dimensional Layered Double Hydroxide Nanosheet Array/Graphene Composite: Fabrication and High Supercapacitor Performance. *J. Mater. Chem. A* **2014,** *2*, 1022-1031.

(12) Jiang, Z.; Li, Z.; Qin, Z.; Sun, H.; Jiao, X.; Chen, D., LDH Nanocages Synthesized with MOF Templates and Their High Performance as Supercapacitors. *Nanoscale* **2013,** *5*, 11770-11775.
(13) Hu, H.; Guan, B.; Xia, B.; Lou, X. W., Designed Formation of Co_3O_4/$NiCo_2O_4$ Double-Shelled Nanocages with Enhanced Pseudocapacitive and Electrocatalytic Properties. *J. Am. Chem. Soc.* **2015,** *137*, 5590-5595.
(14) Qiu, S.; Wang, X.; Yu, B.; Feng, X.; Mu, X.; Yuen, R. K. K.; Hu, Y., Flame-Retardant-Wrapped Polyphosphazene Nanotubes: A Novel Strategy for Enhancing the Flame Retardancy and Smoke Toxicity Suppression of Epoxy Resins. *J. Hazard. Mater.* **2017,** *325*, 327-339.
(15) Qiu, S.; Xing, W.; Feng, X.; Yu, B.; Mu, X.; Yuen, R. K. K.; Hu, Y., Self-Standing Cuprous Oxide Nanoparticles on Silica@ Polyphosphazene Nanospheres: 3D Nanostructure for Enhancing the Flame Retardancy and Toxic Effluents Elimination of Epoxy Resins Via Synergistic Catalytic Effect. *Chem. Eng. J.* **2017,** *309*, 802-814.
(16) Pan, Y.-T.; Zhang, L.; Zhao, X.; Wang, D.-Y., Interfacial Engineering of Renewable Metal Organic Framework Derived Honeycomb-Like Nanoporous Aluminum Hydroxide with Tunable Porosity. *Chem. Sci.* **2017,** *8*, 3399-3409.
(17) Hummers Jr, W. S.; Offeman, R. E., Preparation of Graphitic Oxide. *J. Am. Chem. Soc.* **1958,** *80*, 1339-1339.
(18) Han, X.; Yu, C.; Yang, J.; Zhao, C.; Huang, H.; Liu, Z.; Ajayan, P. M.; Qiu, J., Mass and Charge Transfer Coenhanced Oxygen Evolution Behaviors in CoFe-Layered Double Hydroxide Assembled on Graphene. *Adv. Mater. Interfaces* **2016,** *3*, 1500782.
(19) Chen, H.; Hu, L.; Chen, M.; Yan, Y.; Wu, L., Nickel‐Cobalt Layered Double Hydroxide Nanosheets for High‐Performance Supercapacitor Electrode Materials. *Adv. Funct. Mater.* **2014,** *24*, 934-942.
(20) Jiang, J.; Zhang, A.; Li, L.; Ai, L., Nickel–Cobalt Layered Double Hydroxide Nanosheets as High-Performance Electrocatalyst for Oxygen Evolution Reaction. *J. Power Sources* **2015,** *278*, 445-451.
(21) Teng, Y.; Zhao, H.; Zhang, Z.; Li, Z.; Xia, Q.; Zhang, Y.; Zhao, L.; Du, X.; Du, Z.; Lv, P.; Świerczek, K., Mos_2 Nanosheets Vertically Grown on Graphene Sheets for Lithium-Ion Battery Anodes. *ACS Nano* **2016,** *10*, 8526-8535.
(22) Li, L.; Ma, R.; Ebina, Y.; Fukuda, K.; Takada, K.; Sasaki, T., Layer-by-Layer Assembly and Spontaneous Flocculation of Oppositely Charged Oxide and Hydroxide Nanosheets into Inorganic Sandwich Layered Materials. *J. Am. Chem. Soc.* **2007,** *129*, 8000-8007.
(23) Ma, H.; He, J.; Xiong, D.-B.; Wu, J.; Li, Q.; Dravid, V.; Zhao, Y., Nickel Cobalt Hydroxide@ Reduced Graphene Oxide Hybrid Nanolayers for High Performance Asymmetric Supercapacitors with Remarkable Cycling Stability. *ACS Appl. Mater. Inter.* **2016,** *8*, 1992-2000.
(24) Kang, N.-J.; Wang, D.-Y., A Green Functional Nanohybrid: Preparation, Characterization and Properties of a B-Cyclodextrin Based Functional Layered Double Hydroxide. *J. Mater. Chem. A* **2013,** *1*, 11376-11383.
(25) Zhang, L.; Zhang, X.; Shen, L.; Gao, B.; Hao, L.; Lu, X.; Zhang, F.; Ding, B.; Yuan, C., Enhanced High-Current Capacitive Behavior of Graphene/CoAl-Layered Double Hydroxide Composites as Electrode Material for Supercapacitors. *J. Power Sources* **2012,** *199*, 395-401.
(26) Zhou, L.; Xu, J.; Miao, H.; Wang, F.; Li, X., Catalytic Oxidation of Cyclohexane to Cyclohexanol and Cyclohexanone over Co_3O_4 Nanocrystals with Molecular Oxygen. *Appl. Catal. A - Gen.* **2005,** *292*, 223-228.

(27) Hu, Z.-A.; Xie, Y.-L.; Wang, Y.-X.; Wu, H.-Y.; Yang, Y.-Y.; Zhang, Z.-Y., Synthesis and Electrochemical Characterization of Mesoporous Co_xNi_{1-x} Layered Double Hydroxides as Electrode Materials for Supercapacitors. *Electrochim. Acta* **2009,** *54*, 2737-2741.
(28) Wu, Y.; Shi, Q.; Li, Y.; Lai, Z.; Yu, H.; Wang, H.; Peng, F., Nitrogen-Doped Graphene-Supported Cobalt Carbonitride@Oxide Core-Shell Nanoparticles as a Non-Noble Metal Electrocatalyst for an Oxygen Reduction Reaction. *J. Mater. Chem. A* **2015,** *3*, 1142-1151.
(29) Lee, J. W.; Ahn, T.; Soundararajan, D.; Ko, J. M.; Kim, J.-D., Non-Aqueous Approach to the Preparation of Reduced Graphene Oxide/A-$Ni(Oh)_2$ Hybrid Composites and Their High Capacitance Behavior. *Chem. Commun.* **2011,** *47*, 6305-6307.
(30) Ma, R.; Liang, J.; Takada, K.; Sasaki, T., Topochemical Synthesis of Co-Fe Layered Double Hydroxides at Varied Fe/Co Ratios: Unique Intercalation of Triiodide and Its Profound Effect. *J. Am. Chem. Soc.* **2010,** *133*, 613-620 %@ 0002-7863.
(31) Yang, J.; Yu, C.; Fan, X.; Zhao, C.; Qiu, J., Ultrafast Self-Assembly of Graphene Oxide-Induced Monolithic NiCo-Carbonate Hydroxide Nanowire Architectures with a Superior Volumetric Capacitance for Supercapacitors. *Adv. Funct. Mater.* **2015,** *25*, 2109-2116.
(32) Kim, P.; Shi, L.; Majumdar, A.; McEuen, P. L., Thermal Transport Measurements of Individual Multiwalled Nanotubes. *Phys. Rev. Lett.* **2001,** *87*, 215502.
(33) Hu, M.; Shenogin, S.; Keblinski, P., Molecular Dynamics Simulation of Interfacial Thermal Conductance between Silicon and Amorphous Polyethylene. *Appl. Phys. Lett.* **2007,** *91*, 241910.
(34) Si, Y.; Samulski, E. T., Exfoliated Graphene Separated by Platinum Nanoparticles. *Chem. Mater.* **2008,** *20*, 6792-6797.
(35) Song, P. a.; Yu, Y.; Zhang, T.; Fu, S.; Fang, Z.; Wu, Q., Permeability, Viscoelasticity, and Flammability Performances and Their Relationship to Polymer Nanocomposites. *Ind. Eng. Chem. Res.* **2012,** *51*, 7255-7263.
(36) Wen, X.; Gong, J.; Yu, H.; Liu, Z.; Wan, D.; Liu, J.; Jiang, Z.; Tang, T., Catalyzing Carbonization of Poly (L-Lactide) by Nanosized Carbon Black Combined with Ni_2o_3 for Improving Flame Retardancy. *J. Mater. Chem. A* **2012,** *22*, 19974-19980.
(37) Zhang, J.; Kong, Q.; Yang, L.; Wang, D.-Y., Few Layered $Co(Oh)_2$ Ultrathin Nanosheet-Based Polyurethane Nanocomposites with Reduced Fire Hazard: From Eco-Friendly Flame Retardance to Sustainable Recycling. *Green Chem.* **2016**.
(38) Wang, D.-Y.; Das, A.; Costa, F. R.; Leuteritz, A.; Wang, Y.-Z.; Wagenknecht, U.; Heinrich, G., Synthesis of Organo Cobalt− Aluminum Layered Double Hydroxide Via a Novel Single-Step Self-Assembling Method and Its Use as Flame Retardant Nanofiller in Pp. *Langmuir* **2010,** *26*, 14162-14169.
(39) Shan, X.; Song, L.; Xing, W.; Hu, Y.; Lo, S., Effect of Nickel-Containing Layered Double Hydroxides and Cyclophosphazene Compound on the Thermal Stability and Flame Retardancy of Poly (Lactic Acid). *Ind. Eng. Chem. Res.* **2012,** *51*, 13037-13045.
(40) Kalali, E. N.; Wang, X.; Wang, D.-Y., Multifunctional Intercalation in Layered Double Hydroxide: Toward Multifunctional Nanohybrids for Epoxy Resin. *J. Mater. Chem. A* **2016,** *4*, 2147-2157.
(41) Cao, Y.; Feng, J.; Wu, P., Preparation of Organically Dispersible Graphene Nanosheet Powders through a Lyophilization Method and Their Poly (Lactic Acid) Composites. *Carbon* **2010,** *48*, 3834-3839.
(42) Qiu, S.; Xing, W.; Mu, X.; Feng, X.; Ma, C.; Yuen, R. K. K.; Hu, Y., A 3D Nanostructure Based on Transition Metal Phosphide Decorated Heteroatom-Doped Mesoporous Nanospheres Interconnected with Graphene: Synthesis and Applications. *ACS Appl. Mater. Inter.* **2016,** *8*, 32528-32540.

(43) Zhu, J.; Wei, S.; Ryu, J.; Budhathoki, M.; Liang, G.; Guo, Z., In Situ Stabilized Carbon Nanofiber (Cnf) Reinforced Epoxy Nanocomposites. *J. Mater. Chem. A* **2010,** *20*, 4937-4948.
(44) Bao, C.; Guo, Y.; Song, L.; Kan, Y.; Qian, X.; Hu, Y., In Situ Preparation of Functionalized Graphene Oxide/Epoxy Nanocomposites with Effective Reinforcements. *J. Mater. Chem. A* **2011,** *21*, 13290-13298.
(45) Ash, B. J.; Siegel, R. W.; Schadler, L. S., Mechanical Behavior of Alumina/Poly(Methyl Methacrylate) Nanocomposites. *Macromolecules* **2004,** *37*, 1358-1369.
(46) Qian, M.; Sun, Y.; Xu, X.; Liu, L.; Song, P.; Yu, Y.; Wang, H.; Qian, J., 2D-Alumina Platelets Enhance Mechanical and Abrasion Properties of Pa612 Via Interfacial Hydrogen-Bond Interactions. *Chem. Eng. J.* **2017,** *308*, 760-771.
(47) Gu, H.; Guo, J.; He, Q.; Tadakamalla, S.; Zhang, X.; Yan, X.; Huang, Y.; Colorado, H. A.; Wei, S.; Guo, Z., Flame-Retardant Epoxy Resin Nanocomposites Reinforced with Polyaniline-Stabilized Silica Nanoparticles. *Ind. Eng. Chem. Res.* **2013,** *52*, 7718-7728.

Table of Contents Graphic

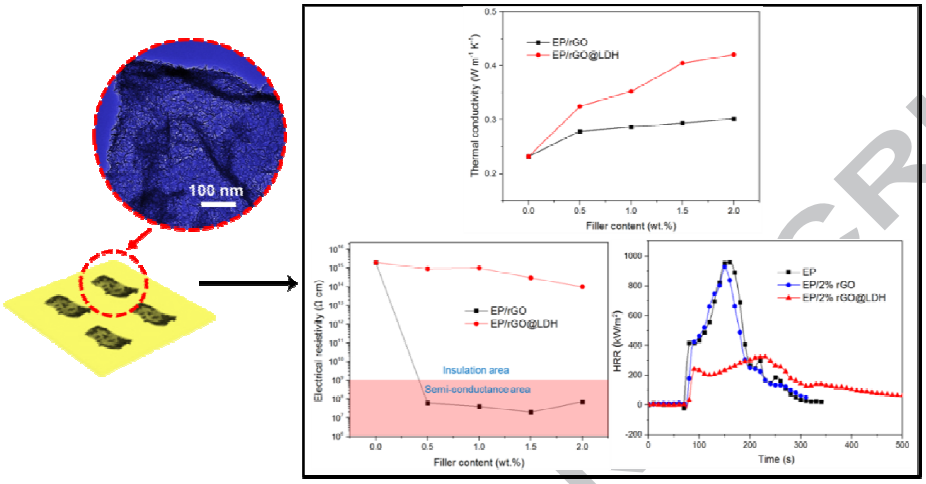

Highlights

- MOF-derived LDH nanosheets were anchored onto graphene via “3D fabrication method”.
- LDH nanosheets lying or standing on the graphene constructed a unique sandwich structure.
- The hybrid was incorporated into epoxy resin to improve its thermal conductivity.
- The hybrid endowed flame retardancy to the epoxy nanocomposite without sacrificing the electrical insulation.